Proceedings of 17th International Symposium on Plasma Chemistry, Toronto, Canada, August 7-12, 2005

Effect of Oxygen Injection into Argon Induction Plasmas on Chemically Non-Equilibrium Conditions

Nobuhiko Atsuchi[1], Masaya Shigeta[2], and Takayuki Watanabe[2]

[1] *Department of Nuclear Engineering, Tokyo Institute of Technology, Tokyo, Japan*
[2] *Department of Environmental Chemistry and Engineering, Tokyo Institute of Technology, Yokohama, Japan*

Abstract
Effective generation of chemical reactive species in thermal plasmas has been required in the field of material processing and waste treatment. The effect of oxygen injection into argon induction plasmas was investigated by numerical analysis without chemical equilibrium assumptions for the dissociation and ionization. Oxygen dissociation and heat flux to torch wall can be controlled by oxygen injection location. Therefore, suitable oxygen injection needs to be chosen according to the application requirement.

1. Introduction

Thermal plasmas have been used for a number of applications of material processing and waste treatment. In these applications, effective generation of chemical reactive species is required. The modeling of induction thermal plasmas with several injection methods of nitrogen or hydrogen was performed previously [1]. The purpose of this work is to investigate the effect of oxygen injection into argon induction plasmas on chemically non-equilibrium (CNE) conditions by numerical analysis. Reaction kinetics rates of the dissociation and recombination of oxygen as well as the ionization were taken into account in this modeling. The transport properties were estimated using higher-order approximation of Chapman-Enskog method [2].

2. Numerical formulation

2-1 Thermodynamic and transport properties

Higher-order approximation of the Chapman-Enskog method is used according to the required accuracy for transport properties. Modeling of induction thermal plasmas has been performed with the first-order approximation because higher-order of Sonine polynomial expansion requires many kinds of collision integrals resulting in the complex formula. The first-order approximation may cause errors especially for electrical conductivity and thermal conductivity of electron translational contribution over 10000 K [3]. The collision integrals were taken from Ref. [4-11] which provide intermolecular potential and fitting data. Detailed descriptions of the calculation method of viscosity, thermal conductivity and electrical conductivity are given by Watanabe and Sugimoto [3]. In CNE model, the transport and thermodynamic properties are related to the temperature and the composition of plasmas. Therefore, the transport and thermodynamic properties should be estimated considering the diffusion of species in plasmas at each calculation step until the convergence.

The thermodynamic properties, enthalpy and specific heat at constant pressure, were obtained from the equilibrium properties. This would be oversimplification, however, the exact estimation of the non-equilibrium thermodynamics properties is very complex to satisfy the self-consistent conditions. The radiative intensity of argon and oxygen was taken from Ref. [12-13].

2-2 Kinetic rate constants

The equilibrium composition was estimated by FACT (Center for Research in Computational Thermochemistry), considering six species of Ar, Ar^+, O_2, O, O^+, and e^-. Table 1 summarizes the reactions of Ar-O_2 mixture considered in this study. Twelve reactions comprising 6 forward reactions in Table 1 and their backward reactions were taken into account. The reaction rates for forward direction are given by Arrhenius equation.

Table 1 Chemical reactions in argon-oxygen mixtures.

Reaction	a_l	b_l	c_l
$O_2 + O_2 \rightarrow O + O + O_2$	2.0×10^{21}	-1.5	59500
$O_2 + O \rightarrow O + O + O$	1.0×10^{22}	-1.5	59500
$O_2 + Ar \rightarrow O + O + Ar$	1.0×10^{22}	-1.5	59500
$O_2 + e^- \rightarrow O + O + e^-$	9.68×10^{22}	-2.0	59500
$O + e^- \rightarrow O^+ + e^- + e^-$	3.91×10^{33}	-3.78	158500
$Ar + e^- \rightarrow Ar^+ + e^- + e^-$	k_l^f was calculated by Eq. (2)		

$$k_l^f = a_l T^{b_l} \exp(-c_l / T) \tag{1}$$

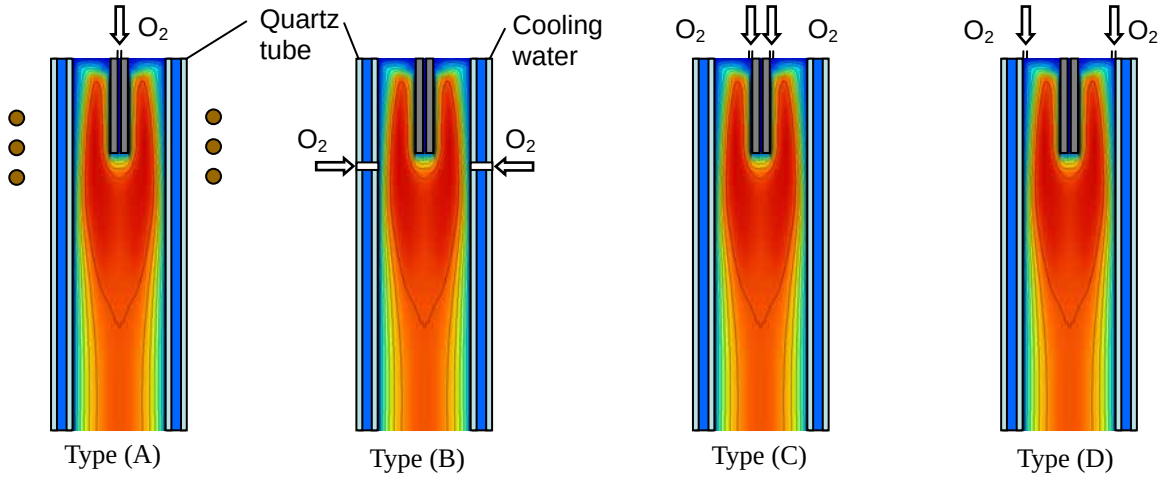

Fig. 1 Schematic diagram of oxygen injection location types.

For Ar ionization reaction, the reaction rate can be calculated by Eq. (2) [14].

$$k_l^f = 1.68\times10^{-20}T^{1.5}(135300/T+2)\exp(-135300/T) \tag{2}$$

2-4 Calculation model

Four injection locations of oxygen were considered in the modeling as illustrated in Fig. 1; (A) center injection; (B) radial injection at the center of the coil; (C) inner injection from the top; (D) sheath gas injection.

The geometry of calculation domain of induction plasma torch is shown in Fig. 2 and the operating conditions are summarized in Table 2. Gas flow rate of each oxygen injection type was shown in Table 3. The plasma torch consists of a water-cooled quartz tube, and is surrounded by a water-cooled induction coil. The coil consists of three turns and applies the induction frequency at 4 MHz to the plasma. The actual power level was assumed to be 5 kW.

The calculation are based on the following assumptions to derive the governing equations: (a) steady-state laminar flow; (b) axial symmetry; (c) optically thin; (d) negligible viscous dissipation in energy equation; (e) negligible displacement current in comparison with the conductive current; (f) negligible flow-induced electric field; (g) same temperature of heavy particles and electrons.

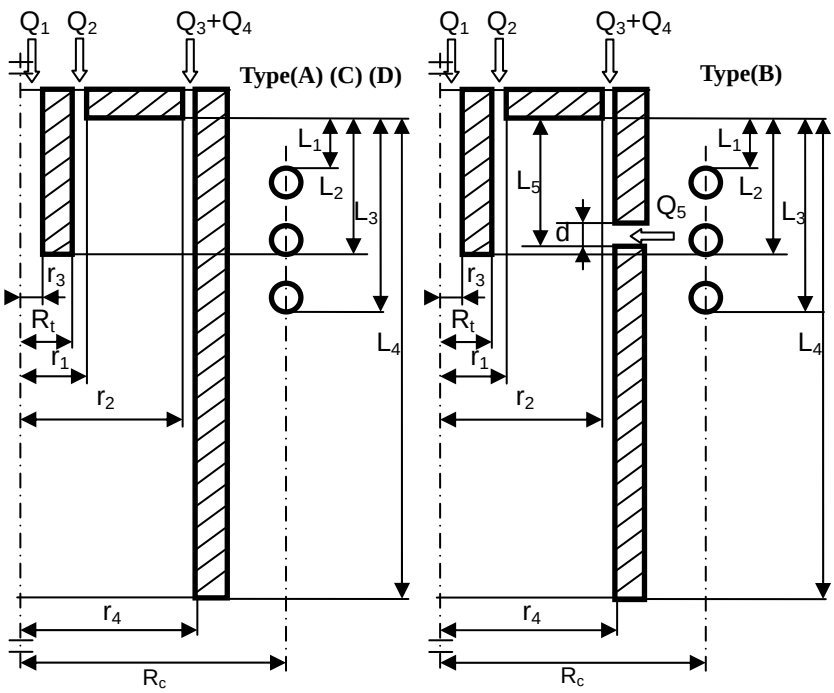

Fig. 2 Geometry of calculation domain of induction plasma torch.

Table 2 Torch characteristic dimensions and operational condition.

Torch Power	5 kW
Work Frequency	4 MHz
Reactor Pressure	101.3 kPa
Coil Radius	32 mm
Coil turn number	3
Wall thickness	1.5 mm
L_1	19 mm
L_2	45 mm
L_3	65 mm
L_4	190 mm
L_5	40 mm
r_1	6.5mm
r_2	21 mm
r_3	1 mm
r_4	22.5 mm
R_t	4.5 mm
d	0.1 mm

The effect of turbulence has been reported by Chen and Boulos [15]. They reported that most of the flow field in induction plasmas was laminar at the Reynolds number 625 at the gas inlet, while the turbulence effect is large at the Reynolds number 3125. The flow field of the present induction plasmas can be considered as laminar, because the inlet Reynolds number is 350 in this study.

Table 3 Flow rate of each injection type.

(L/min)	Type (A)	Type (B)	Type (C)	Type (D)
Q1	**O_2: 0.1**	0	0	0
Q2	3	3	3 (**O_2: 0.1**)	3
Q3 + Q4	26.9	24	27	27(**O_2: 1**)
Q5	-	**O_2: 3**	-	-
Total	30	30	30	30

2-5 Governing equations and boundary conditions

The field of flow, temperature and concentration in induction thermal plasmas were calculated by solving the two-dimensional continuity, momentum, energy, and species conservation equations coupled with the Maxwell's equations. Reactions of the dissociation and recombination as well as the ionization were taken into account in this modeling.

Continuity:

$$\nabla \cdot (\rho \mathbf{u}) = 0 \tag{3}$$

Momentum:

$$\rho \mathbf{u} \cdot \nabla \mathbf{u} = -\nabla p + \nabla \tau + \mathbf{J} \times \mathbf{B} \tag{4}$$

Energy:

$$\rho \mathbf{u} \cdot \nabla h = \nabla \cdot \left(\frac{\lambda}{C_p} \nabla h \right) + \mathbf{J} \cdot \mathbf{E} - q_r \tag{5}$$

Species:

$$\rho \mathbf{u} \cdot \nabla Y_i = \nabla \cdot (\rho D \nabla Y_i) + R_{ri} \tag{7}$$

Electromagnetic:

$$\nabla^2 \mathbf{E} - \xi \sigma \frac{\partial \mathbf{E}}{\partial t} = 0 \tag{8}$$

The boundary conditions along the centerline were set to insure axial symmetry. At the wall of the plasma torch, no slip conditions are maintained for the velocity, and the concentrations have zero gradient. The temperature at the inside wall of the plasma torch was calculated assuming that the outside wall was maintained at 300 K by water cooling. The injection tube was assumed to be at 500 K. The outflow boundary conditions at the torch were assumed that the gradient of the variables are zero. The sheath gas has swirl velocity component. Each gas stream has constant axial velocity with zero radial velocity having temperature at 300 K.

2-5 Calculation procedure

The governing conservation equations were solved using SIMPLER (Semi-Implicit Method for Pressure Linked Equation Revised) algorithm [16]. The governing equations and the electric field intensity equation with the associated boundary conditions were discretized into finite difference from using control-volume technique. In oxygen injection types (A), (C), and (D), non-uniform grid points 30 by 30 were used for radial and axial directions, respectively. In oxygen injection type (B), non-uniform grid points 30 by 54 were used for radial and axial directions, respectively. Grids are made finer close to the center and the coil region. Thermodynamic and transport properties were calculated from the temperature and compositions at each position in the calculation domain at each iteration step.

3. Result and discussion

The effect of oxygen injection of type (A: center injection) on plasma characteristics is presented in Fig. 3. At the oxygen injection region, the temperature decreases due to oxygen dissociation as shown in Fig. 3 (a). Higher heat capacity including oxygen dissociation approximately 4000 K leads to a decrease in the plasma temperature. The flow field in Fig. 3 (b) exhibits the characteristic recirculation caused by the radial Lorentz force above the coil region. The corresponding concentration profiles of oxygen atoms and molecules are illustrated in Fig. 3 (c) and (d), respectively. Injected oxygen molecules are dissociated quickly because oxygen is injected directly into the high-temperature region. Therefore, dissociated oxygen

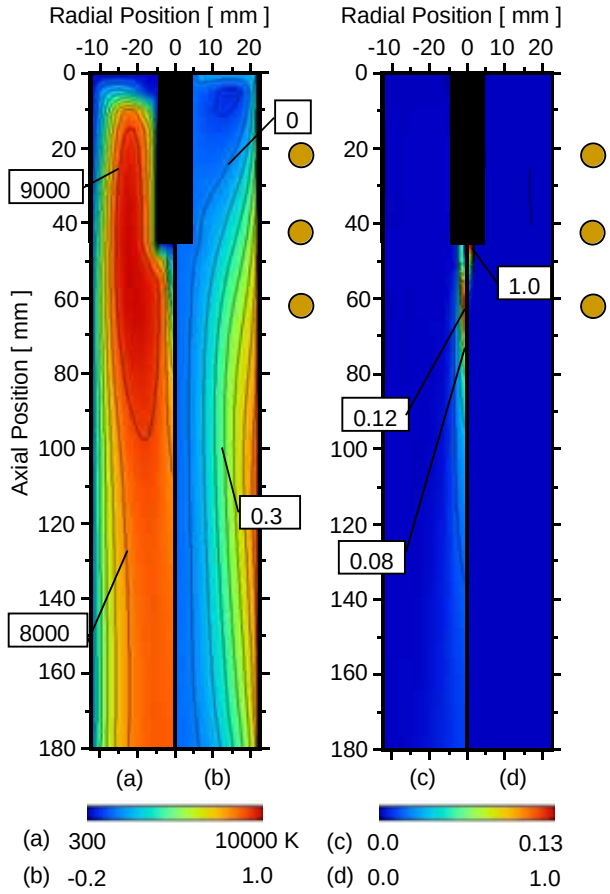

Fig. 3 (a) Isotherms, (b) streamlines, (c) O atom concentration, and (d) O_2 concentration distributions in an Ar-O_2 plasma; Type (A): center injection at 0.1 L/min.

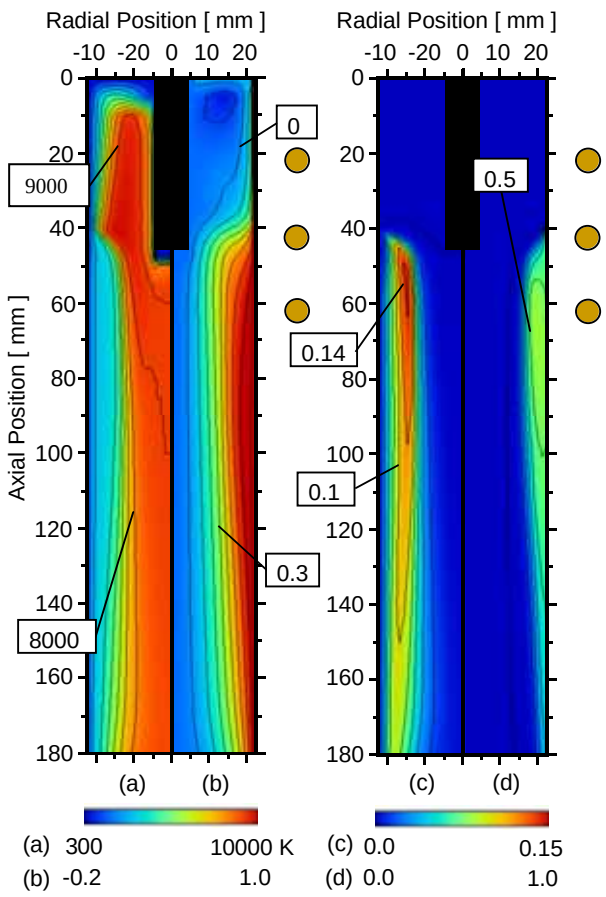

Fig. 4 (a) Isotherms, (b) streamlines, (c) O atom concentration, and (d) O_2 concentration distributions in an Ar-O_2 plasma; Type (B): radial injection at 3 L/min.

atoms can be found near the center of the torch.

Numerical results of oxygen injection type (B: radial injection) is shown in Fig. 4. The calculated temperature field in Fig. 4 (a) shows the severe decrease in temperature at the oxygen injection region along the torch wall due to oxygen dissociation. The streamlines shown in Fig. 4 (b) demonstrate the modified flow field from other injection types in the coil region because of the radial injection toward the high-temperature region. The concentration profiles of oxygen atoms and molecules are presented in Fig. 4 (c) and (d), respectively. Oxygen molecules and dissociated oxygen atoms exist locally near the torch wall owing to the negligible diffusion of dissociated oxygen atoms toward the torch center.

The temperature field in Fig. 5 (a) and the flow field in Fig. 5 (b) in the case of oxygen injection type (C: inner injection) are comparable to types (A) and (D). Thus, the effect of inner injection from the top is weak on the plasma characteristics. The corresponding concentration profiles of oxygen atoms in Fig. 5 (c) and molecules in Fig. 5 (d) indicate that injected oxygen molecules are dissociated quickly above the coil region. Dissociated oxygen atoms exist broadly except the low-temperature region near the torch wall. The widespread mixing of oxygen is due to the recirculation caused by the Lorentz force in the coil region.

The effect of oxygen injection type (D: sheath gas injection) is presented in Fig. 6. High-temperature region above 8000 K is almost the same with an argon plasma, while the temperature decreases slightly near the torch wall region as shown in Fig. 6 (a). The concentration profiles of oxygen atoms and molecules are shown in Fig. 6 (c) and (d), respectively. Injected oxygen molecules exist near the torch wall through the downstream region. The dissociated oxygen atoms exist broadly to the torch center owing to the recirculation. Oxygen injection from the top of the torch results in the broad distribution of dissociated oxygen atoms.

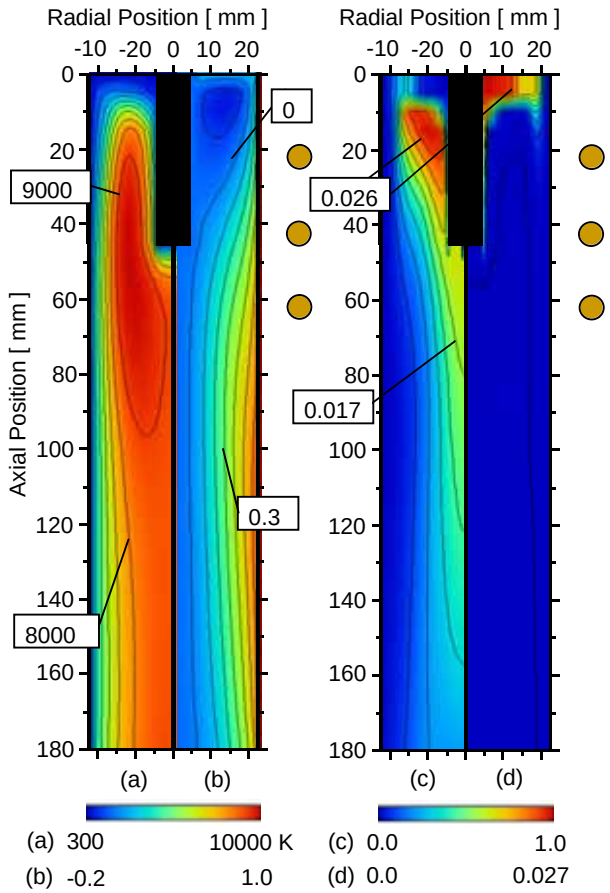

Fig. 5 (a) Isotherms, (b) streamlines, (c) O atom concentration, and (d) O_2 concentration distributions in an Ar-O_2 plasma; Type (C): inner injection at 0.1 L/min.

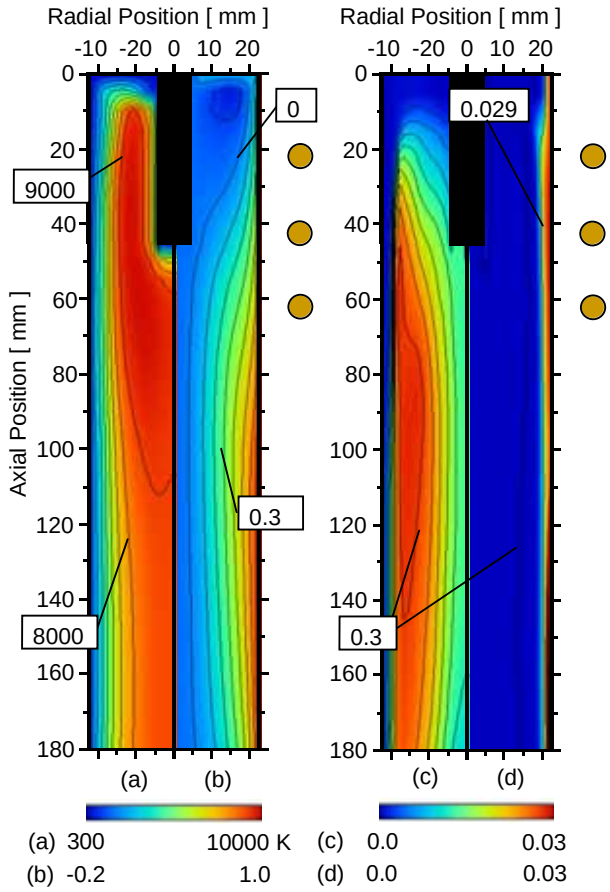

Fig. 6 (a) Isotherms, (b) streamlines, (c) O atom concentration, and (d) O_2 concentration distributions in an Ar-O_2 plasma; Type (D): sheath gas injection at 1 L/min.

Degree of CNE, δ, was introduced to evaluate chemical non-equilibrium of plasmas.

$$\text{Degree of CNE for dissociation:} \quad \delta^{d}_{O_2} = \frac{[O]^2}{[O_2]K_d} \tag{9}$$

$$\text{Degree of CNE for ionization:} \quad \delta^{i}_{O} = \frac{[O^+][e^-]}{[O]K_i} \tag{10}$$

In these definitions, value of $\delta = 1$ represents complete equilibrium. In non-equilibrium, $\delta > 1$ represents overpopulation of products and underpopulation of reactants for $\delta < 1$.

Fig. 7 presents the radial profiles of the degree of CNE due to dissociation of injected oxygen with type (B) at the center of the coil. The degree of CNE deviates strongly from the equilibrium value at the oxygen injection region. This indicates that the chemical non-equilibrium occurs at the injection region due to the effect of diffusion and finite reaction rate. In the downstream region, the chemical non-equilibrium occurs near the torch wall. In all injection types, the strong chemical non-equilibrium was found at the oxygen injection region and near the torch wall where the concentration gradient is high.

Fig. 8 shows the effect of oxygen injection on axial profiles of the degree of dissociation. High degree of dissociation is obtained by oxygen injection types (A) and (C). The high degree of dissociation in types (A) and (C) is attributed to the direct oxygen injection into the high-temperature region of plasmas. While, the degree of dissociation is low in the case of types (B) and (D), because oxygen molecules exist locally near the torch wall. Oxygen injection type (B) which is direct radial injection from the torch wall provides the lowest degree of dissociation. The lowest degree of dissociation results from the insufficient penetration of

injected oxygen into the high-temperature region of plasmas, therefore higher injection velocity is required to obtain higher degree of dissociation of oxygen.

Fig. 9 presents the effect of oxygen injection on axial profiles of heat flux to the torch wall. The low heat flux in the coil region in type (B) and (D) is due to the large amount oxygen flow along the torch wall, resulting in the severe decrease in the temperature. In contrast, the heat flux to the torch wall in type (A) and (C) is high. The contribution of the center or inner oxygen injection is small for lowering the heat flux to the torch wall by the oxygen injection.

Non-equilibrium modeling with finite reaction rates for various oxygen injection locations demonstrates the following results; chemical non-equilibrium exists at the region of high-concentration gradient such as oxygen injection region and near the torch wall. The degree of dissociation of oxygen and the heat flux to torch wall can be controlled by oxygen injection location. Therefore, suitable oxygen injection location needs to be chosen according to the application requirements. The present modeling would give the guidance for the rational design of new material processing with effective reactive gas injection into plasmas.

4. References

[1] T. Watanabe, T. Honda, and A. Kanzawa Proc. ISPC-10, 1.1-31, Bochum (1991)

[2] J. O. Hirschfelder, C. F. Curtiss, and R. B. Bird, Molecular Theory of Gases and Liquids, John Wiley, New York, (1964)

[3] T. Watanabe and N. Sugimoto, Thin Solid Films, **457**, 201 (2004)

[4] E. Mason, J. Chem. Phys., **22**,169 (1954)

[5] L. Monchick, Phys. Fluids, **2**, 695 (1959)

[6] T. Kihara, et al., Phys. Fluids, **3**, 715 (1960)

[7] F. Smith, et al., J. Chem. Phys., **41**, 3560 (1964)

[8] R. Devoto, Phys. Fluids, **10**, 354 (1967)

[9] H. Milloy, Aust. J. Phys., **30**, 61 (1977)

[10] M. Capitelli, et al., J. Thermophys., **14**, 259 (2000)

[11]J. Aubreton, C. Bonnefoi, and J. M. Mexmain, Rev. Phys Appl., **21**, 365 (1986)

[12] R. Krey and J. Morris, Phys. Fluids, **13**, 1483 (1970)

[13] R. Miller and R. Ayen, J. Appl. Phys., **40**, 5260 (1969)

[14] M. I. Hoffert and H. Lien, Phys. Fluids, **10**, 1769 (1967)

[15] K. Chen and M. I. Boulos, J. Phys. D: Appl. Phys. **27**, 946 (1994)

[16] S. V. Patanker, Numerical Heat and Fluid Flow, McGraw-Hill, New York, (1980)

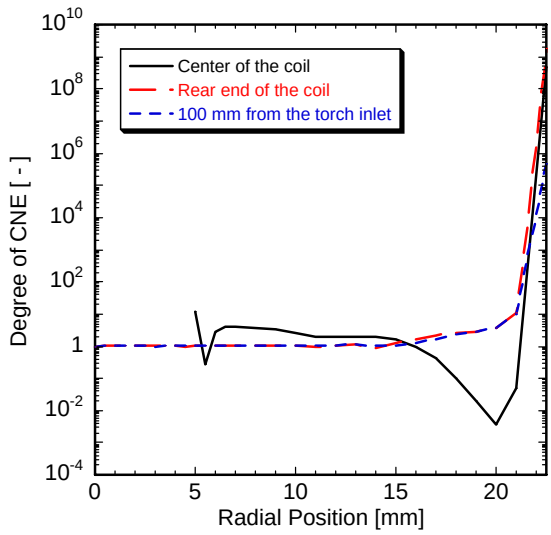

Fig. 7 Radial profiles of degree of CNE due to dissociation; (B) radial injection.

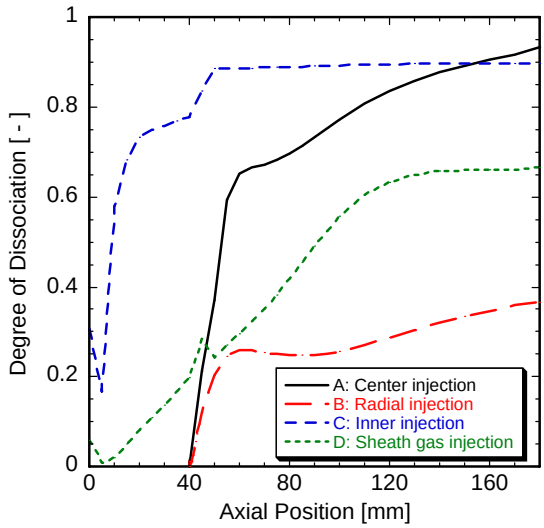

Fig. 8 Effect of oxygen injection on axial profiles of degree of dissociation.

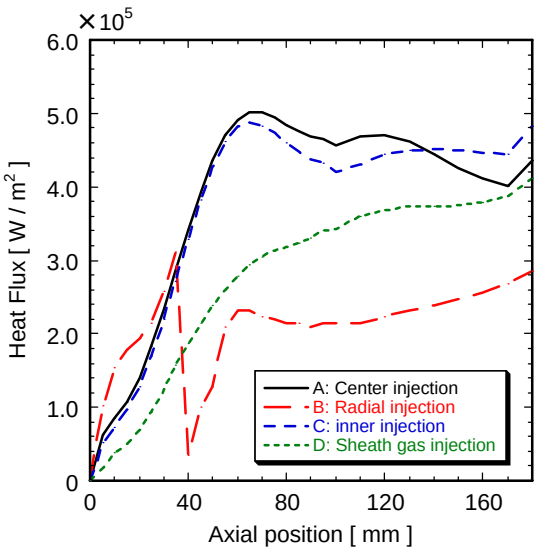

Fig. 9 Effect of oxygen injection on axial profiles of heat flux to torch wall.